PAPER G

RADON TRANSFORM / GAUSSIAN BEAM MIGRATION

Spyros K. Lazaratos and Jerry M. Harris
Seismic Tomography Project

ABSTRACT

Migration algorithms usually treat each point in the subsurface as an isolated diffractor. Yet, dicrete point diffractors are rare; reflections from continuous beds usually dominate the data. Regions of the subsurface could be adequately imaged through the use of a limited range of dips around a dominant local dip. It is often the case that several migrations will be performed, in order to select the optimal velocity model that will produce a well focused image. In this case an estimate of the local dip will be available after the first migration. Subsequent migrations could be very efficient, if this estimate could be incorporated into the imaging algorithm.

Motivated by this observation we derived a migration algorithm based on the reconstruction of the image from its dip spectrum. In more formal terms, we form an image by inverting its Radon transform. The Radon transform is formed by applying appropriate stacking operators to the data.

The Radon transform is a global concept. In order to be able to treat different areas of the image independently and migrate through general velocity models, we need to localize our imaging principle. We achieve this through the use of Gaussian beam wavefields as a basis for imaging. This represents an intermediate approach between point source wavefields, forming the basis for Kirchoff migration, and plane waves associated with slant-stack migrations.

The implementation of the algorithm is efficient. The subsurface can be imaged through the use of sparse fans of rays, each of them effectively imaging the neighbourhood of its origin. So, although the algorithm represents a bottom-up approach, excessive ray tracing is avoided.

The ability of the algorithm to image portions of the subsurface with relatively few rays and the possibility to concentrate on specific dips might have interesting applications in the optimization of the velocity model used for migration.

INTRODUCTION

In recent years there has been renewed interest in the use of ray methods for the solution of the seismic inverse problem (Clayton and Stolt (1981), Carter and Frazer (1984), Stolt and Weglein (1985), Cohen, Hagin and Bleistein (1985), Bleistein, Cohen and Hagin (1987), Bleistein (1987), Beydoun and Keho (1987), Keho and Beydoun (1988), Beydoun and Mendes (1989), Ikelle (1989)). The work of Beylkin has been

In the above definition A is the spreading-free amplitude defined as

$$A = (\frac{v_0\rho_0}{v\rho})^{1/2} v_0^{1/2} \tag{2}$$

where v,ρ are the velocity and density and v_0,ρ_0 their values at the point where the initial conditions for the beam (width, curvature) are specified. The quantity Q is a complex solution of the dynamic ray tracing equations. It is a complex spreading, describing both amplitude change and phase change. So, as the beam propagates and spreads, both the amplitude and the wavelet change. The traveltime τ is complex

$$\tau = \tau_r + i\tau_i \tag{3}$$

The real part of the traveltime is given by the paraxial approximation

$$\tau_r(\vec{r}) = \tau_0(\vec{r}_0) + \frac{1}{2} M_R x^2 \tag{4}$$

where $\tau_0(\vec{r}_0)$ is the traveltime at the projection $\vec{r}_0$ on the ray of the point $\vec{r}$ (see Figure 1), x is the distance of $\vec{r}$ from the ray and M_R is the curvature of the wavefront defined from the initial curvature and width of the beam through the solution of the dynamic ray tracing equations. The form of the last equation shows that the wavefronts of Gaussian beams are parabolic. The imaginary part of the traveltime is given by

$$\tau_i(\vec{r}) = \frac{1}{2} M_I x^2 \tag{5}$$

where the imaginary curvature M_I is also defined through the dynamic ray tracing equations. So the imaginary traveltime is parabolic and its exponential is a Gaussian, hence the name Gaussian beams. An excellent reference on Gaussian beams and dynamic ray tracing is the paper by Červený (1985).

Gaussian beams are generally presented in the frequency domain. In fact the amplitude decay of a Gaussian beam away from the central ray is Gaussian only for a fixed frequency. Since Gaussian beam wavefields are the basis for our algorithm, and time domain images of Gaussian beam wavefields are not common in the literature, we show a few examples in Figure 2.

RADON TRANSFORM

We give here the expressions for the 2-D Radon transform and its inverse, mainly to introduce the notation that we are going to use. The Radon transform $\hat{f}(\vec{p},l)$ of a 2-D function $f(\vec{r})$ is formed by the line integrals of $f(\vec{r})$ along straight lines, identified by their direction (defined by the normal unit vector $\vec{p}$) and their distance from the origin l. So:

$$\hat{f}(\vec{p},l) = \int d\vec{r} f(\vec{r}) \delta(l - \vec{p}\vec{r}) \tag{6}$$

The inverse of the Radon transform is

$$f(\vec{r}) = \frac{1}{4\pi} R(\vec{r}) * \int_0^{2\pi} dp \hat{f}(\vec{p}, l = \vec{p}\vec{r}) \tag{7}$$

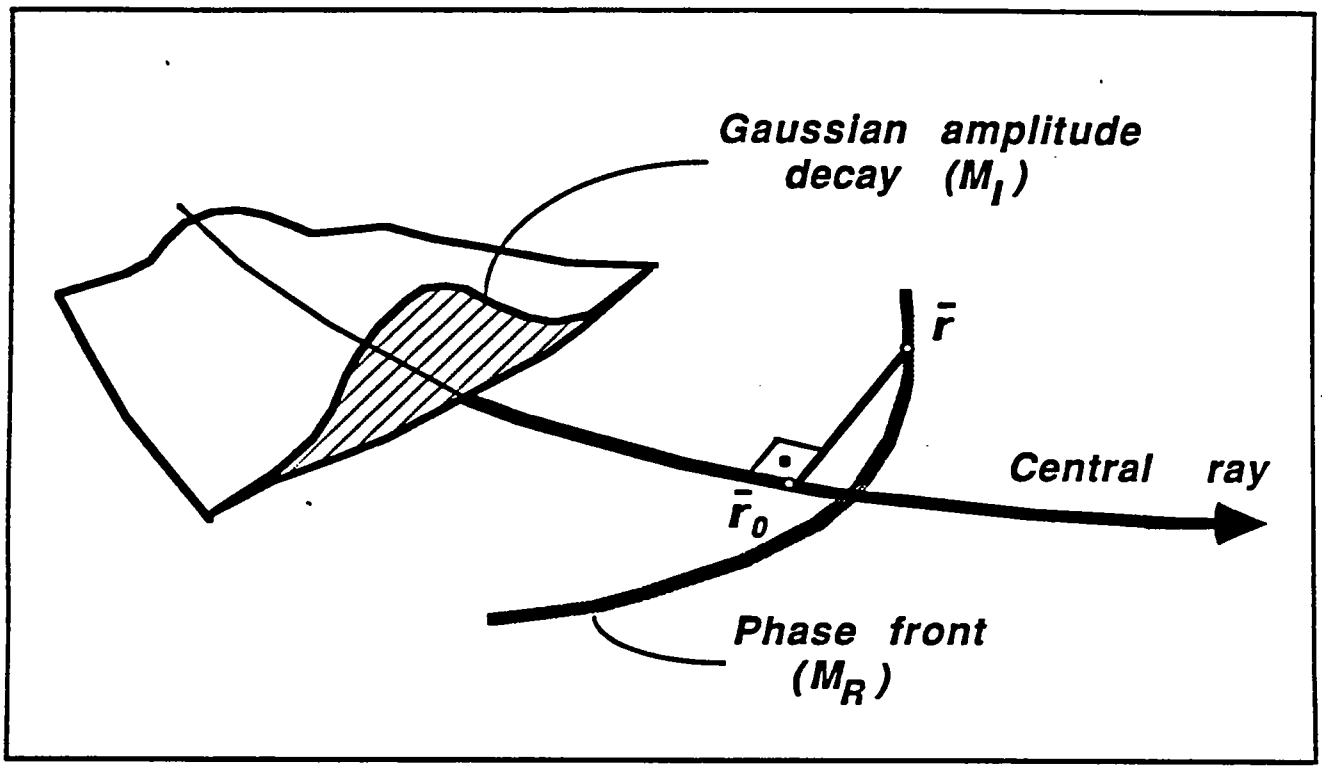

Figure 1. Gaussian beams

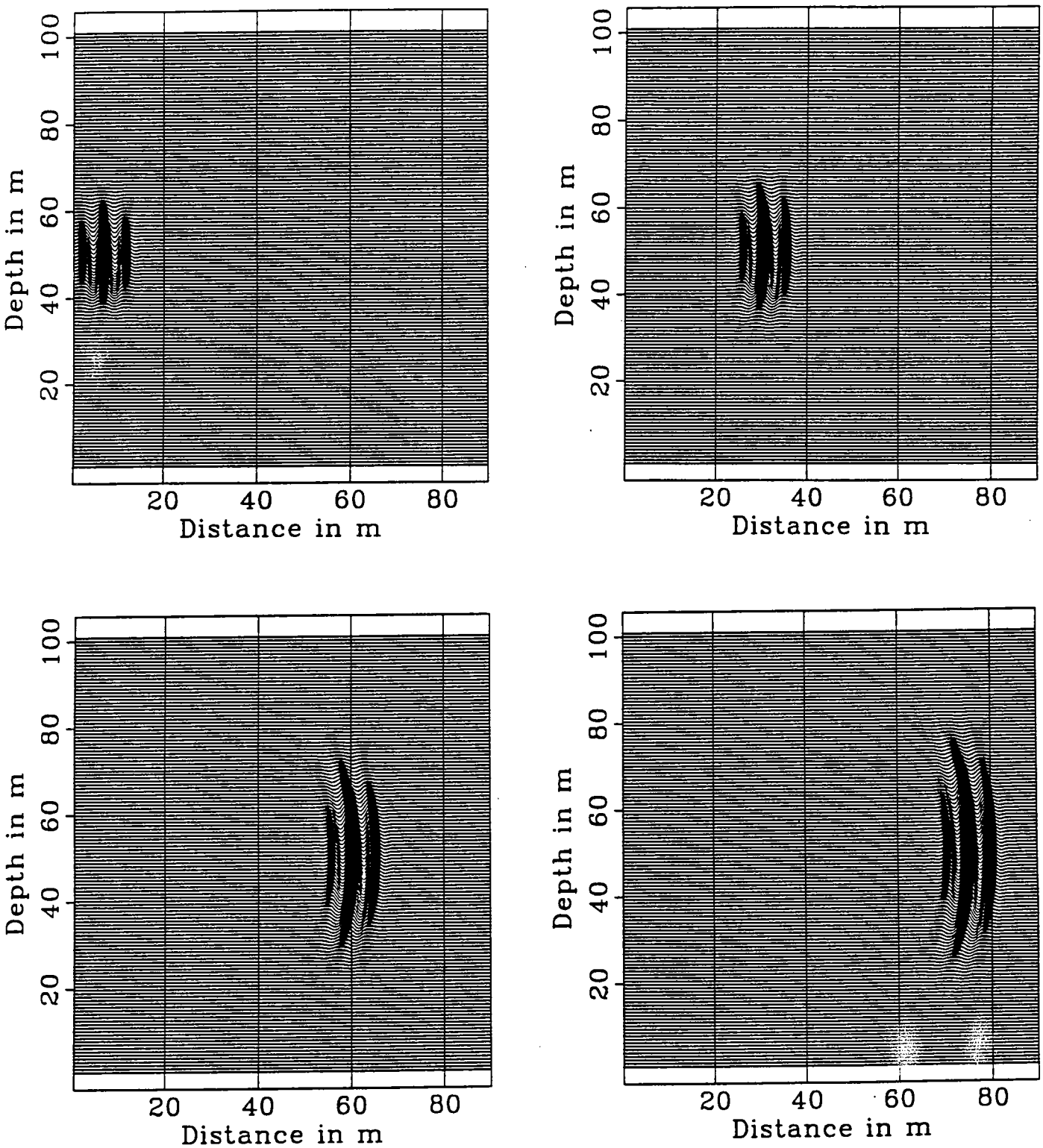

Figure 2. Snapshots of a propagating Gaussian beam. The wavefield has been calculated from a single horizontal ray.

where $*$ denotes convolution and $R(\vec{r})$ is the two-dimensional rho-filter (a spatial filter whose frequency response is $\sqrt{k_x^2 + k_z^2}$).

HOW TO SAMPLE THE RADON TRANSFORM

Since the Radon transform can be inverted, it follows that, if we can form the Radon transform of the image from the data, we have essentially solved the imaging problem. In this section we describe the appropriate way to operate on the data in order to sample the Radon transform.

To simplify the presentation we are going to describe the zero offset case, corresponding to CDP stacked data. We are going to outline the generalization to pre-stack migration in a later section.

We base our derivation on the Kirchoff integral (Schneider (1978), Berkhout (1981)), which allows us to calculate the scattered wavefield from its values at the surface. For a constant density acoustic medium the appropriate expression is

$$U_s(\vec{r};\omega) = \frac{1}{4\pi}\int [U_s(\vec{r}_R;\omega)\frac{\partial G_0(\vec{r};\vec{r}_R;\omega)}{\partial z_R} - \frac{\partial U_s(\vec{r}_R;\omega)}{\partial z_R} G_0(\vec{r};\vec{r}_R;\omega)]d\vec{r}_R \qquad (8)$$

In the above equation $U_s(\vec{r};\omega)$ is the scattered wavefield at point $\vec{r}$ of the subsurface; $U_s(\vec{r}_R;\omega)$ is the scattered wavefield recorded at the location $\vec{r}_R$ on the surface. The Green's function $G_0(\vec{r};\vec{r}_R;\omega)$ represents the pressure field recorded at surface location $\vec{r}_R$ due to a monopole at $\vec{r}$. The partial derivative with respect to z_R is the partial derivative in the direction normal to the receiver line, which, for simplicity, is assumed to be the line $z = 0$.

According to the exploding reflector imaging principle the image of the subsurface is given by the value of the scattered wavefield at time zero. If we call $f(\vec{r})$ this image, representing the result of migration, we have

$$f(\vec{r}) = \frac{1}{4\pi}\int d\omega \int d\vec{r}_R [U_s(\vec{r}_R;\omega)\frac{\partial G_0(\vec{r};\vec{r}_R;\omega)}{\partial z_R} - \frac{\partial U_s(\vec{r}_R;\omega)}{\partial z_R} G_0(\vec{r};\vec{r}_R;\omega)] \qquad (9)$$

The Radon transform of the image $f(\vec{r})$ is then

$$\hat{f}(\vec{p},l) = \frac{1}{4\pi}\int d\omega \int d\vec{r}_R [U_s(\vec{r}_R;\omega)\frac{\partial W_{\vec{p},l}(\vec{r}_R;\omega)}{\partial z_R} - \frac{\partial U_s(\vec{r}_R;\omega)}{\partial z_R} W_{\vec{p},l}(\vec{r}_R;\omega)] \qquad (10)$$

where the quantity

$$W_{\vec{p},l}(\vec{r}_R;\omega) = \int d\vec{r} G_0(\vec{r};\vec{r}_R;\omega)\delta(l - \vec{p}\vec{r}) \qquad (11)$$

is the wavefield at the surface due to a plane wave source located into the medium along a line whose orientation is given by the unit vector $\vec{p}$ and whose distance from the origin is l (see Figure 3). In Appendix A we show that a high-frequency, far-field approximation to equation (10) is

$$\hat{f}(\vec{p},l) = \frac{1}{2\pi}\int d\omega \int d\vec{r}_R U_s(\vec{r}_R;\omega)\frac{\cos\theta(\vec{r}_R)}{v(\vec{r}_R)}[-i\omega W_{\vec{p},l}(\vec{r}_R;\omega)] \qquad (12)$$

where $\theta(\vec{r}_R)$ is the angle formed by the normal to the wavefront of $W_{\vec{p},l}$ and the vertical. The quantity $\cos\theta(\vec{r}_R)$ is an obliquity factor similar to the one encountered in Kirchoff migration.

So, in order to find the value of the line integral along the image, we need to

1. Calculate the wavefield $W_{\vec{p},l}(\vec{r}_R;\omega)$.

2. Apply to the data the stacking operator

$$\int d\omega \int d\vec{r}_R S_{\vec{p},l}(\vec{r}_R;\omega) \tag{13}$$

where

$$S_{\vec{p},l}(\vec{r}_R;\omega) = \frac{1}{2\pi}\frac{\cos\theta(\vec{r}_R)}{v(\vec{r}_R)}[-i\omega W_{\vec{p},l}(\vec{r}_R;\omega)] \tag{14}$$

In a homogeneous or layered velocity background it is easy to propagate a plane wavefield. This is the basic idea behind $\tau - p$ domain inversions and Fourier domain algorithms like the phase shift and $f - k$ migrations. Diffraction tomography algorithms (Devaney (1984), Harris (1987)) are also generally formulated in the Fourier domain. Yet, when lateral variation is introduced in the velocity model, originally plane wavefields do not propagate in a simple way. We propose to handle the propagation issue by decomposing the plane wavefields into a superposition of Gaussian beams.

The fact that Gaussian beams can be used as a basis for the synthesis of wavefields has been established through the work of Červený and his co-workers (Červený, Popov and Pšenčik (1982), Červený and Pšenčik (1983), Červený (1983), Červený (1985), Červený (1985a)). Klimeš (1984) showed how a high frequency time-harmonic wavefield specified on an initial surface can be expanded into a sum of Gaussian beams. Raz (1987) proposed the Gabor transformation as a way of performing this decomposition.

Our basic idea of decomposing into Gaussian beams the originally plane wavefields which sample the Radon transform of the medium is shown schematically in Figure 3. In a laterally varying medium the originally plane wavefield arrives at the surface having a different shape. We essentially propose to use spatially limited parabolic wavefields (the Gaussian beams) to approximate this wavefield. The exact way this decomposition is carried out and the resulting imaging algorithm are the subject of the next two sections.

GAUSSIAN BEAM WAVEFIELDS AS A BASIS FOR IMAGING

The inverse of the Radon transform given in equation (7) can be written as

$$f(\vec{r}) = \frac{1}{4\pi}R(\vec{r}) * \int d\vec{p}\int dl\delta(l - \vec{p}\vec{r})\hat{f}(\vec{p},l) \tag{15}$$

The δ function appearing in the last expression can be viewed as the wavefield of a plane wave at a particular instant. We claim that this plane wave wavefield can be

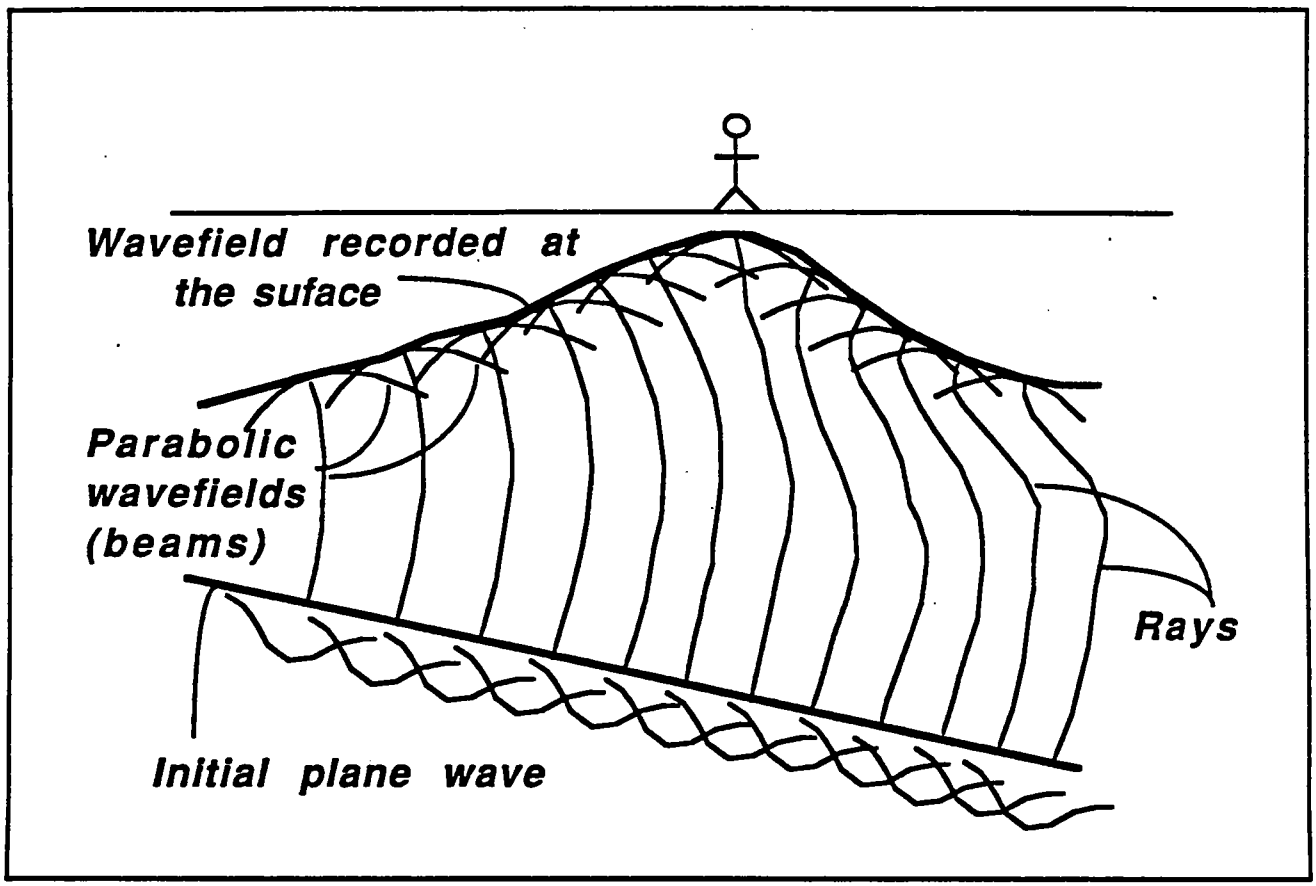

Figure 3. Basic idea for migration algorithm. To find the line integral of the image along a line, we need to calculate the wavefield recorded at the surface when a plane wave source is placed on the line. We calculate this wavefield by decomposing the plane wave into Gaussian beams. This is equivalent to decomposing the wavefield into parabolic wavefields, resulting from the propagation of the Gaussian beams to the surface.

approximated by a sum of Gaussian beam wavefields. We use plane Gaussian beams. An example of the wavefields we use is given in Figure 4. We show a bandlimited wavefield to make it easier to visualize. We are going to use such wavefields as a basis for the construction of the image.

Plane Gaussian beam wavefields are not exactly truncated plane waves. The support of a plane Gaussian beam has some thickness, as shown in Figure 5. Yet, we observed that, when we use beams whose widths are a few times larger than the wavelength for the frequency band of interest, this effect is insignificant (see for example Figure 4). Another approximation we make to simplify the decomposition is to ignore the change in the wavelet as we move away from the central ray. This change occurs because different frequencies attenuate with different rates. The synthetic examples shown later support the fact that these approximations are not severe. We expect that with real data their effect will be much less significant than the effect of noise.

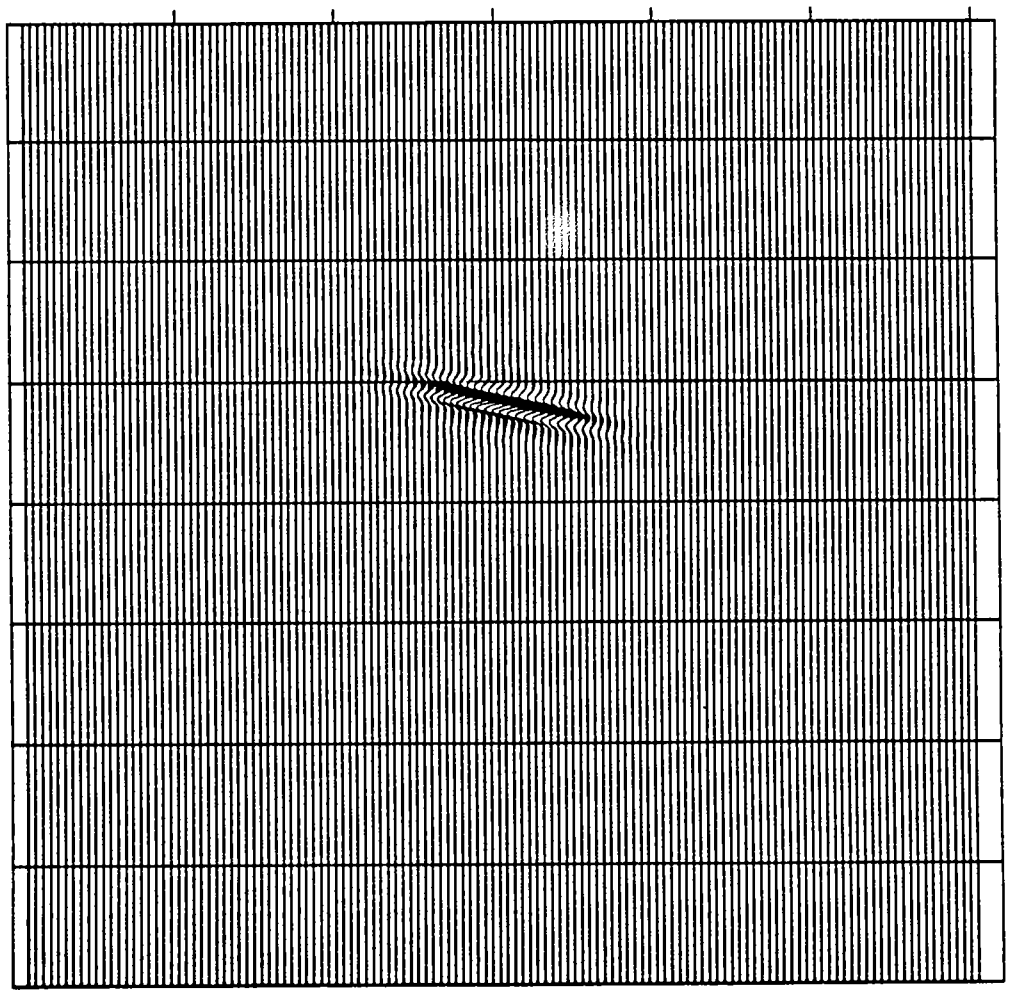

Figure 4. Plane Gaussian beam wavefield. Such wavefields are our basis for imaging.

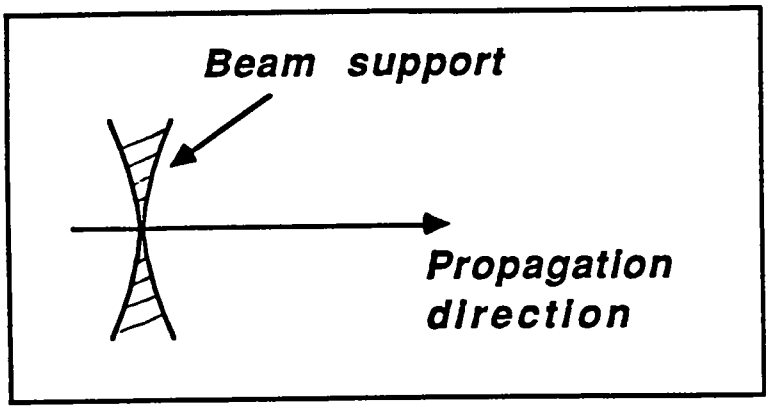

Figure 5. Shape of the support of a plane Gaussian beam wavefield.

So, we essentially approximate the Gaussian beam basis wavefields by short plane waves. The decay away from the central ray is not Gaussian for a bandlimited wavelet. It is Gaussian only for a monochromatic beam. If the spectrum of the wavelet is $S(\omega)$, the decay away from the central ray is

$$\int S(\omega) \exp(-\frac{1}{2}\omega M_I x^2) d\omega \tag{16}$$

where M_I is the imaginary curvature and x the distance from the central ray.

Under the above approximations the decomposition of the plane wavefield into a sum of Gaussian beam wavefields becomes a one dimensional problem. It essentially means the decomposition of a constant function into a sum of functions representing the amplitude tapering of the beams. This can be performed with controlled accuracy, as shown in Figure 6.

Indeed, summing identical translated tapering functions is equivalent to convolving the tapering function with a series of delta functions. In the frequency domain, this means approximating a delta function (the Fourier transform of a constant) by the product of the Fourier transform of the tapering function and a series of delta functions (the Fourier transform of the series of delta functions). We can easily see that we can do that with controlled accuracy provided the tapering has a Fourier transform with effectively finite extent.

We call the Gaussian beam wavefields that form our imaging basis $B_{i,\vec{p},l}(\vec{r})$. The meaning of the indices is shown in Figure 7. The unit vector $\vec{p}$ and the distance from the origin l describe the particular line where the Gaussian beam is originally defined. The index i runs along this line. Beams with the same $\vec{p}$ are originally parallel. Beams with the same l start from the same line.

The decomposition of a plane wave $\delta(l-\vec{p}\vec{r})$ into Gaussian beams, can be described as

$$\delta(l-\vec{p}\vec{r}) = \sum_i B_{i,\vec{p},l}(\vec{r}) \tag{17}$$

Substituting this into equation (15) and approximating the integrations with summations we get

$$f(\vec{r}) = \frac{1}{4\pi} R(\vec{r}) * \sum_{\vec{p}} \sum_l \sum_i \hat{f}(\vec{p},l) B_{i,\vec{p},l}(\vec{r}) \tag{18}$$

This expression suggests that we can write $f(\vec{r})$ in the form

$$f(\vec{r}) = R(\vec{r}) * \sum_{\vec{p}} \sum_l \sum_i a_{i,\vec{p},l} B_{i,\vec{p},l}(\vec{r}) \tag{19}$$

The calculation of the coefficients in this expansion is done through the minimization of a least-squares norm. The derivation is done in Appendix B. The final result of this decomposition is

$$f(\vec{r}) = R(\vec{r}) * \sum_{\vec{p}} \sum_l \sum_i B_{i,\vec{p},l}(\vec{r}) \int d\vec{r} f(\vec{r}) B'_{i,\vec{p},l}(\vec{r}) \tag{20}$$

where

$$B_{i,\vec{p},l}(\vec{r}) = R(\vec{r}) * B'_{i,\vec{p},l}(\vec{r}) \tag{21}$$

Equation (20) is the inversion of the Radon transform in the basis that we introduced. What remains to be done in order to obtain an imaging formula is to show how the integrals in the right hand side of equation (20) can be calculated from the data. This is done in the next section.

THE IMAGING EQUATION

We now show how the coefficients in the expansion of $f(\vec{r})$ given in equation (20) can be calculated from the data. Using again the Kirchoff integral as we did in equations (8) to (12) we can show that

$$\int d\vec{r} f(\vec{r}) B'_{i,\vec{p},l}(\vec{r}) = \int d\vec{r}_R \int d\omega C_{i,\vec{p},l}(\vec{r}_R;\omega) U_s(\vec{r}_R;\omega) \tag{22}$$

where

$$C_{i,\vec{p},l}(\vec{r}_R;\omega) = \frac{1}{2\pi} \frac{\cos\theta(\vec{r}_R)}{v(\vec{r}_R)} [-i\omega W_{i,\vec{p},l}(\vec{r}_R;\omega)] \tag{23}$$

and $W_{i,\vec{p},l}(\vec{r}_R;\omega)$ is the Gaussian beam wavefield at the surface when the wavefield at time zero is $B'_{i,\vec{p},l}(\vec{r})$. It can be calculated through dynamic ray tracing from just one ray. The wavefields $W_{i,\vec{p},l}$ are the spatially limited parabolic wavefields used to approximate the wavefield in Figure 3. So our final imaging equation is:

$$f(\vec{r}) = R(\vec{r}) * \sum_p \sum_l \sum_i B_{i,\vec{p},l}(\vec{r}) \int d\vec{r}_R \int d\omega C_{i,\vec{p},l}(\vec{r}_R;\omega) U_s(\vec{r}_R;\omega) \tag{24}$$

The imaging algorithm described by the last equation works as follows:

- After selecting $B_{i,\vec{p},l}$ (widths and positions of beams to be used) we define $C_{i,\vec{p},l}$ through dynamic ray tracing.
- We stack the data as defined by $C_{i,\vec{p},l}$ and form the quantity

$$\int d\vec{r}_R \int d\omega C_{i,\vec{p},l}(\vec{r}_R;\omega) U_s(\vec{r}_R;\omega) \tag{25}$$

- We spread the above quantity on the image weighting it by $B_{i,\vec{p},l}(\vec{r};\omega)$.
- Repeat for all beams adding all the contributions to form the final image.

In the next section we are going to show how this procedure is actually carried out.

IMPLEMENTATION

We showed before that each component of the Radon transform is defined by the propagation of an initially plane wave to the surface (see Figure 3). This propagation is performed through a group of Gaussian beams, into which the initial plane wave is decomposed. So, we need a very large number of beams to form an image, since we need to sample all the components of the Radon transform (all the combinations of the $\vec{p}$, l parameters). Since every beam requires a central ray, it would seem that our algorithm would require a prohibitively large amount of ray tracing. This is not true. The crucial point about the implementation of the algorithm is that a whole group of beams can be propagated to the surface by just one ray.

We know that, through dynamic ray tracing, a ray defines how a plane Gaussian beam propagates to the surface. In Figure 8a we show the situation. The plane Gaussian beam wavefield is schematically shown as a short linear segment normal to the ray. Yet, this ray contains a lot more information. It also defines how a similar plane Gaussian beam starting at a different position along the ray propagates to the surface. This is shown in Figure 8b. In fact the whole family of plane Gaussian beams starting at different points along the ray can be propagated to the surface through this single ray. This is shown in Figure 8c. Each of those Gaussian beam wavefields is defined by a different linear combination of the two fundamental solutions (point source and plane wave initial conditions) of the dynamic ray tracing equations.

If we shoot a fan of rays, as shown in Figure 8d, we can image an area in the neighbourhood of the center of the fan. The size of the neighbourhood depends on the width of the beams. The rays also give information outside this neighbourhood. Yet, in order to form an image, we need beams intersecting in all possible directions. This is only true around the center of the fan.

The conclusion is that, through a single fan of rays we can image a whole area, the neighbourhood of the fan center. For Kirchoff migration we would need a fan of rays for each image point.

As described in the previous section our migration essentially consists of two basic operations:

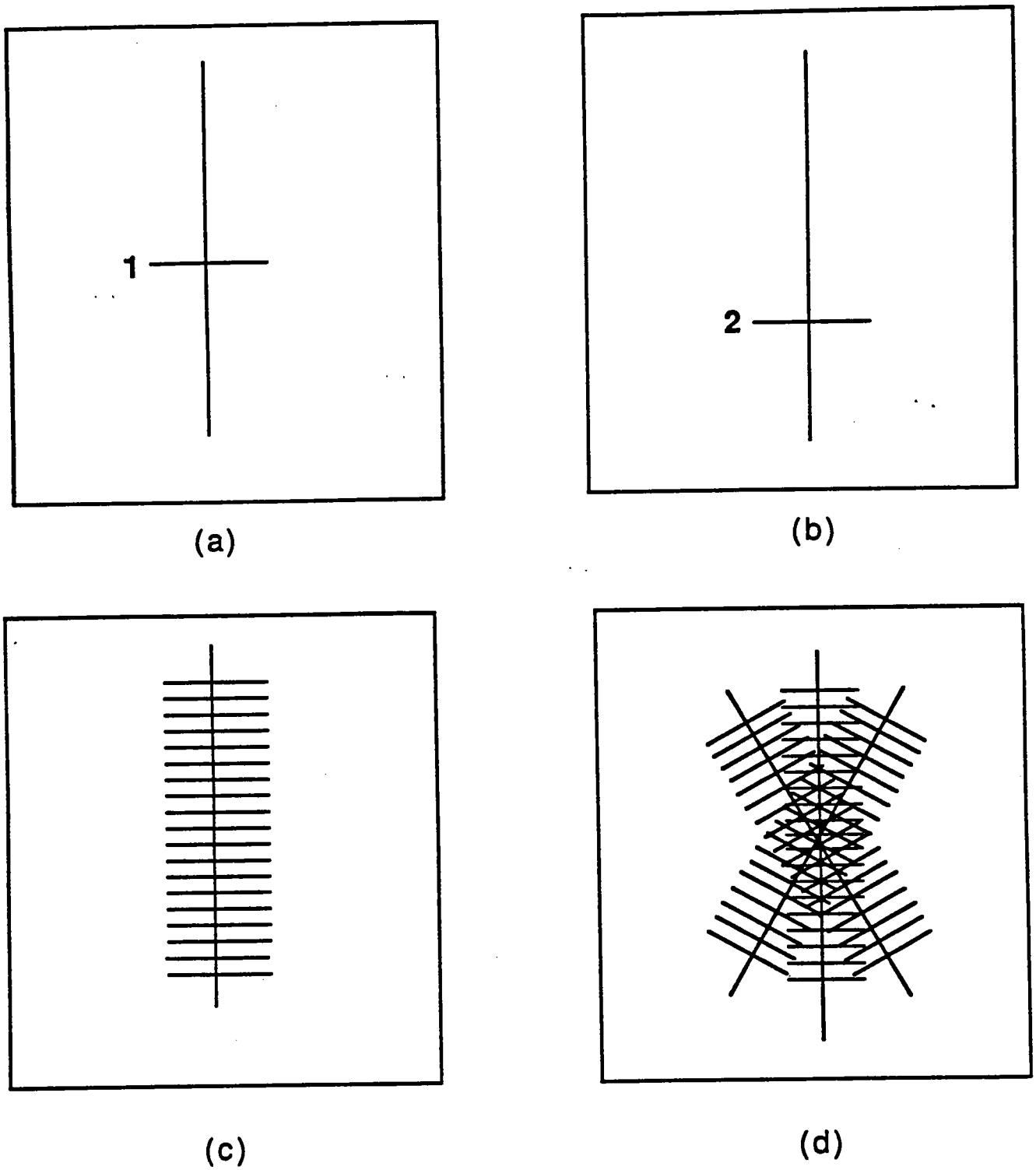

Figure 8. (a) The Gaussian beam starting at position 1 can be propagated to the surface through one central ray. (b) The Gaussian beam starting at position 2 can also be propagated to the surface through the same central ray. (c) In fact a whole group of beams can be propagated to the surface through the same central ray. (d) Imaging through a fan of rays. The neighbourhood of the center can be correctly imaged through this single fan.

- A stacking operation, governed by $C_{i,\vec{p},l}$.
- A spreading operation, governed by $B_{i,\vec{p},l}$.

The stacking operator operates on the data. The result of stacking is spread on the image by the spreading operator. The stacking operator is the wavefield recorded at the receivers when the wavefield at time zero is the wavefield of a single locally plane Gaussian beam given by the spreading operator.

An example of stacking and spreading operators is given in Figures 9 and 10. There is a one-to-one correspondence between the stacking and spreading operators shown in these Figures. Each short linear segment in Figure 9 (a spreading operator) corresponds to a short parabolic segment in Figure 10 (a stacking operator). The spreading operator at the shallowest depth corresponds to the stacking operator at the earliest time. Spreading operators at larger depths correspond to stacking operators at later times. All the stacking/spreading pairs in Figures 9a and 10a have been calculated by a single vertical ray. All the stacking/spreading pairs in Figures 9b and 10b have been calculated by a single ray forming an 8^0 angle with the vertical.

The widths of the stacking and spreading operators are of course related through the wave equation. The spreading operator essentially defines a wavefield on a linear aperture. The rate at which this wavefield spreads depends on the ratio of the wavelength to the size of the aperture. Our objective is to keep the beams as spatially limited as possible. Given the velocity model, the frequency band and a range of depths, we can choose the initial beam width (the width of the spreading operator) in the optimal way, so that the spreading of the beams is minimized.

Let us describe a little bit better the nature and calculation of the stacking and spreading trajectories. Since they represent Gaussian beam wavefields, their frequency content changes as we move away from the central ray. The stacking operation has the form

$$\int d\vec{r}_R \int d\omega \exp(-\omega\tau_i) \exp(i\omega\tau_r) U_s(\vec{r}_R;\omega) \tag{26}$$

where τ_r the real traveltime, calculated by the paraxial approximation and τ_i the imaginary traveltime, proportional to the square of the distance of the receiver from the central ray. In the time domain, the stacking operation becomes

$$\int d\vec{r}_R [U_s(\vec{r}_R;t) * \frac{\tau_i}{t^2+\tau_i^2}]/t = \tau_r \tag{27}$$

When we are close to the central ray $\tau_i \rightarrow 0$ and

$$\frac{\tau_i}{t^2+\tau_i^2} \rightarrow \delta(t) \tag{28}$$

So, the stacking trajectory starts narrow close to the central ray and widens as we move further away. The way we implemented the stacking is the time domain version given in equation (28). We found that, for reasonably broadband wavelets, this was much faster than the usual frequency domain implementation of Gaussian beams, indicated by equation (27).

(a)

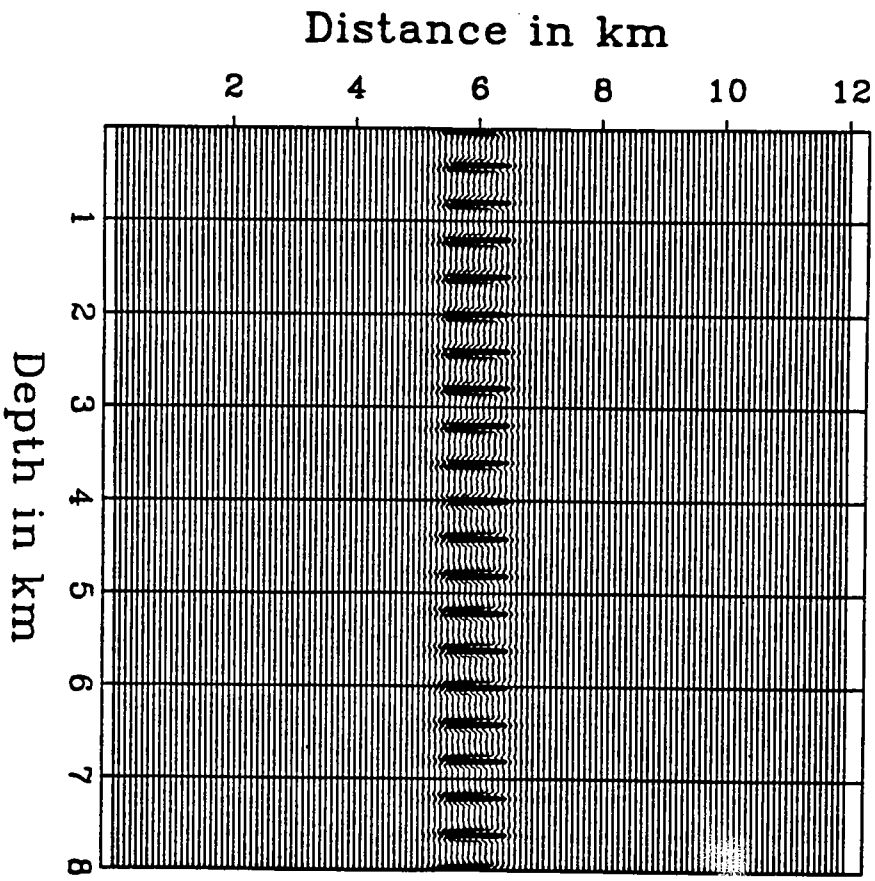

(b)

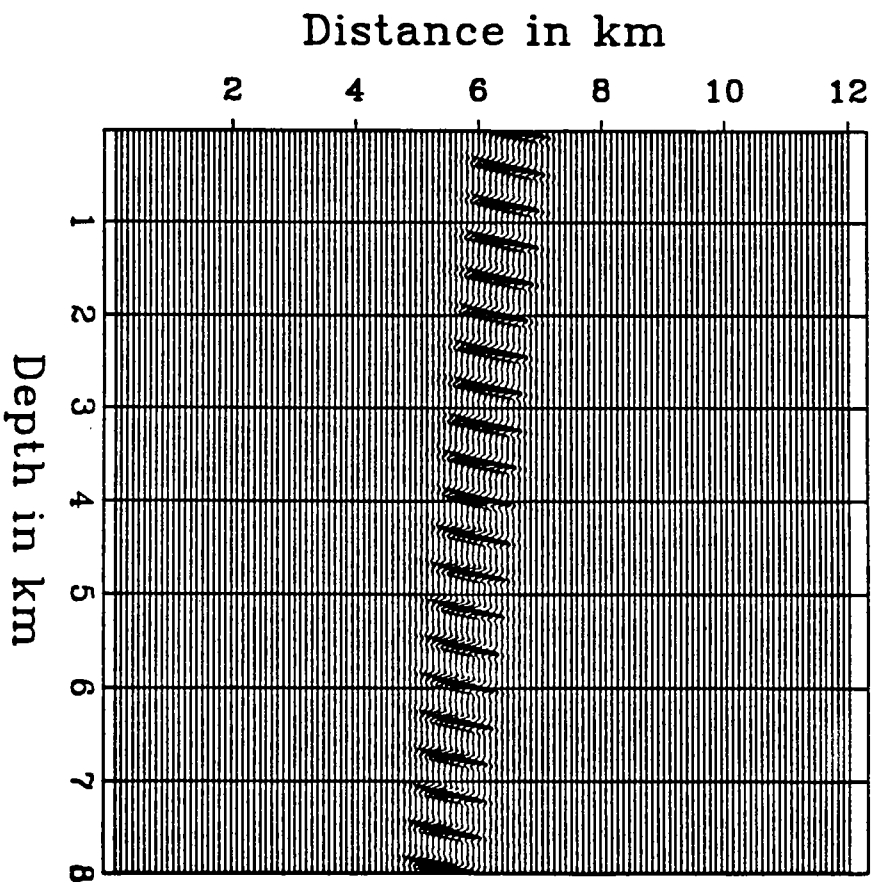

Figure 9. (a). Spreading operators calculated by a vertical ray. (b). Spreading operators calculated by a ray forming an 8^0 angle with the vertical.

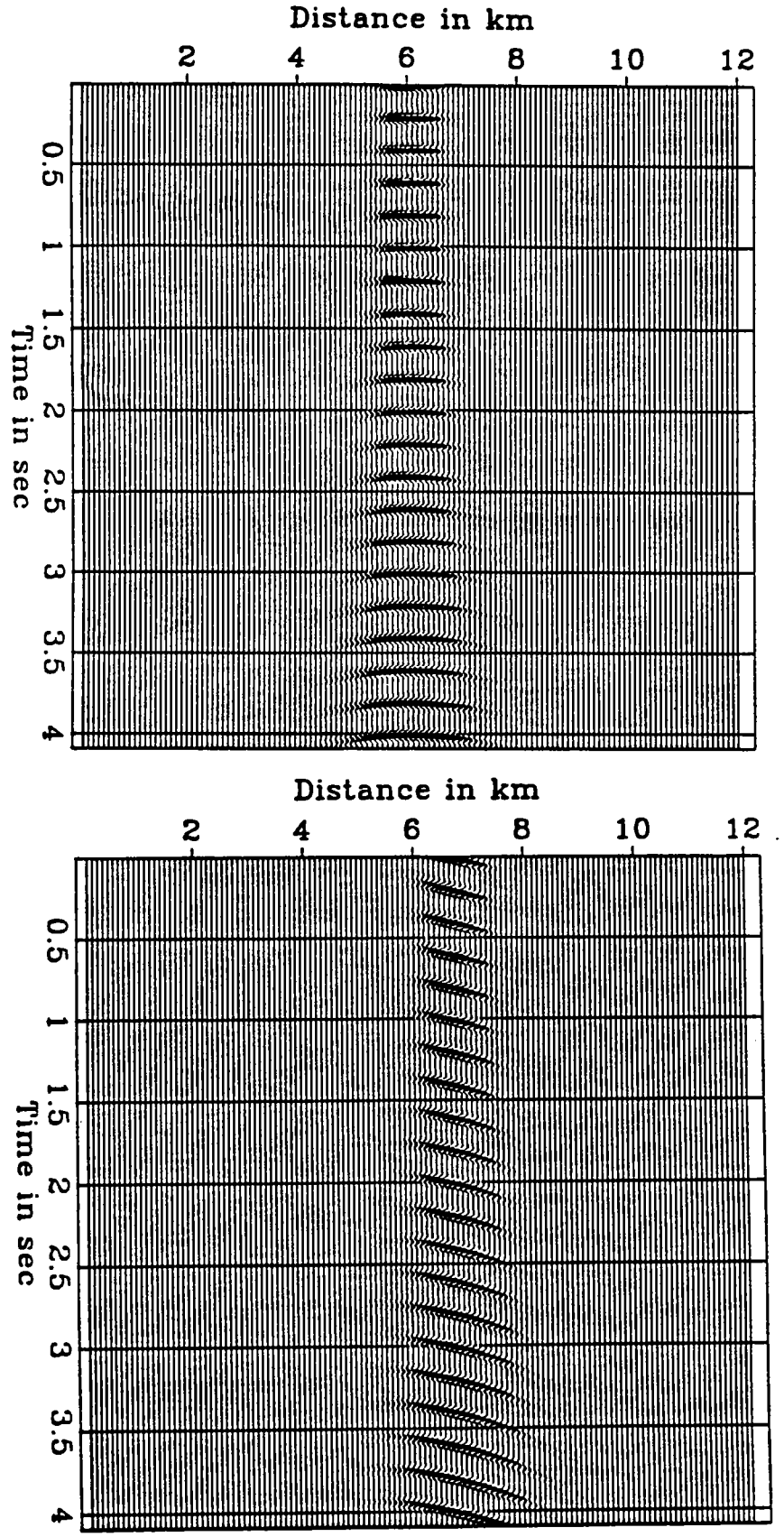

Figure 10. (a). Stacking operators corresponding to the spreading operators in Figure 9a. (b) Stacking operators corresponding to the spreading operators in Figure 9b.

To summarize, our migration works by summing along short parabolic trajectories (which are very close to short hyperbolic trajectories) and spreading the result of the summation along short linear trajectories. The actual way this is implemented is the following:

- From few points in the area of interest we shoot fans of rays.
- Each ray defines a family of stacking trajectories. Stacking the data along these trajectories we create a trace.
- Each ray also defines a family of spreading trajectories. There is a one-to-one correspondence between stacking and spreading trajectories. We spread around the ray along the spreading trajectories the trace generated by stacking.
- We repeat this procedure for all the rays in each fan.
- We combine the images generated by all fans in the way defined by the decomposition of plane waves into Gaussian beams.

PRESTACK MIGRATION

The imaging operator described before extends naturally to the prestack case. In this case, every element of the Radon transform is sampled through two beams: a 'source beam' corresponding to a stacking operation on the sources and a 'receiver beam' corresponding to a stacking operation on the receivers (see Figure 11). The stacking of the sources generates a synthetic source and similarly the stacking of the receivers a synthetic receiver. This synthetic source - synthetic receiver pair samples an element of the Radon transform. This element can be viewed as a reflector. The source beam reflects on this reflector and produces the beam that is received by the synthetic receiver.

Of course there is usually more information about each reflecting element. The same element can be sampled by several synthetic source - synthetic receiver pairs, provided that the geometric requirement of the law of reflection (incidence and reflection angles are equal) is satisfied. In other words there is usually amplitude vs. offset information in the data. The way to use this information to recover the elastic properties of the subsurface under the framework of Born inversion has been shown in Lazaratos (1989).

For the zero-offset case we have seen that the stacking operator implies summing along lines (short pieces of parabolas) in the data space. In the prestack case, the double stack described before (to create the source and receiver beams) implies summing along surfaces in the three-dimensional (source-receiver-time) data cube.

We presented the outline of prestack migration in the source-receiver coordinate system. Through a simple linear transformation we can get to the midpoint-offset coordinate system. Then we would have a 'midpoint beam' and an 'offset beam'.

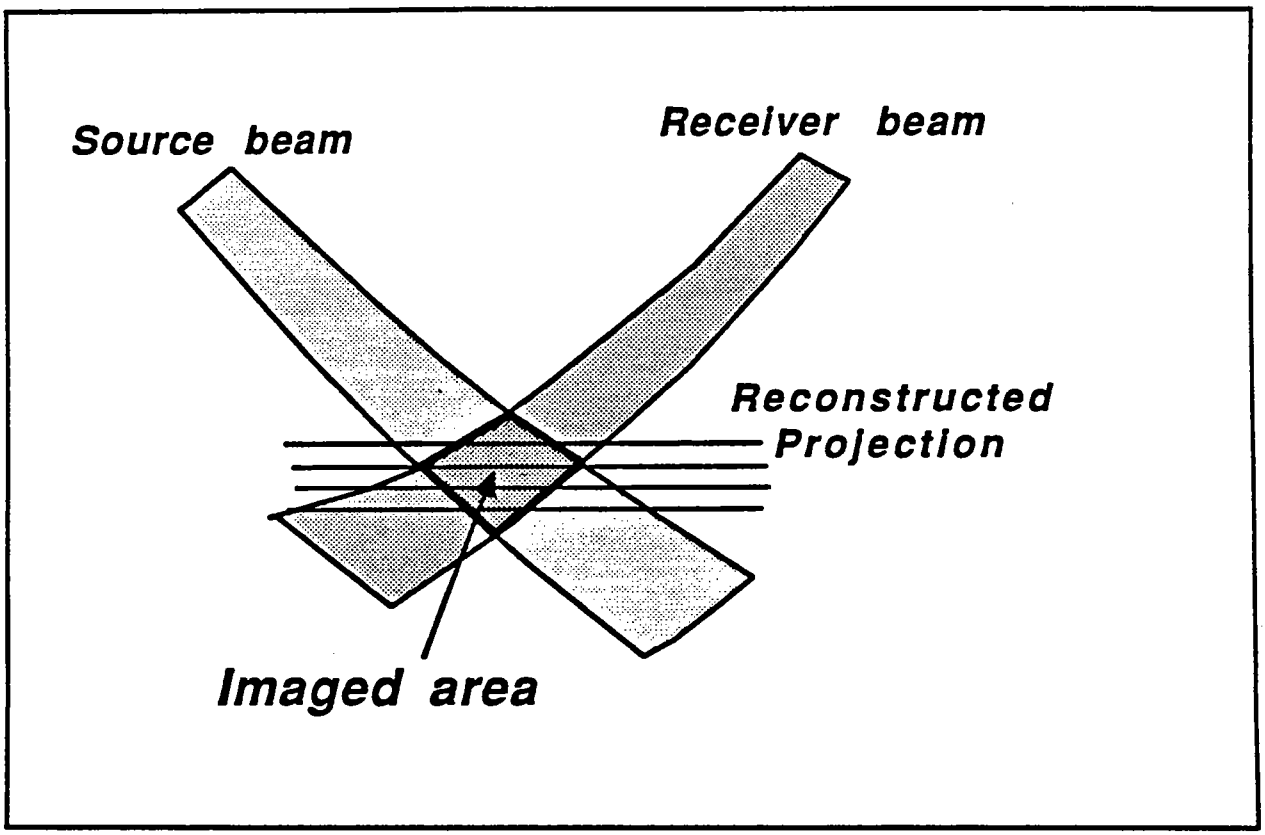

Figure 11. Principle of prestack migration.

The offset beam would be created through a short CDP stack and the midpoint beam through summing along a short parabola, approximating a short hyperbola. So the operation implied by a pair of beams is a partial CDP stack and a partial migration.

The details of the implementation of the prestack version of our migration are a subject of current research.

A SYNTHETIC EXAMPLE

A very simple synthetic example of zero-offset migration is presented in this section. The model is a syncline shown in Figure 12. Synthetic zero-offset data have been generated through the Kirchoff integral. They are shown in Figure 13. A velocity of 4.0 km/s was used. In Figure 15 we show the part of the image constructed through the single ray fan shown in Figure 14. In Figure 17 we show the part of the image constructed through the single ray fan shown in Figure 16. We can see that even a single ray fan images correctly the structure in its neighbourhood. The size of this neighbourhood depends of course on the width of the beams. For these examples the half-width of the beams, for the central frequency of the wavelet, was 1 km in the first case and 2.4 km in the second case.

Of course the amplitudes are not correct. Since the beam fades away from the central ray, the image fades as we move away from the center of the fan. Yet the correct amplitudes can be recovered by combining nearby fans. This part is currently being implemented.

Although the migration has to be tested with more complicated models and velocity backgrounds, we believe that the results from this very simple example are very encouraging. The really important point is that parts of the total image can be reconstructed with relatively few rays. The rays contain the information about the velocity model. They define how the image is affected by changes in the velocity model. Doing the imaging with as few rays as possible means that changes to the image due to changes in the velocity model can be efficiently calculated. We can calculate an exact gradient (of the image with respect to the velocity model) since the effect of each ray on the image is well defined. In the next section we are going to better explain this fact and its possible use for the optimization of the velocity model through which we migrate.

CHARACTERISTICS - POSSIBLE APPLICATIONS

In this section we outline some applications for which our migration algorithm seems to be suitable by its nature. Most of the topics presented below will be the subject of future research.

1. Efficient imaging of restricted areas. One of the things our migration has in common with Kirchoff migration is that the computational effort is inversely proportional to the size of the area that is imaged. This is not true for other types

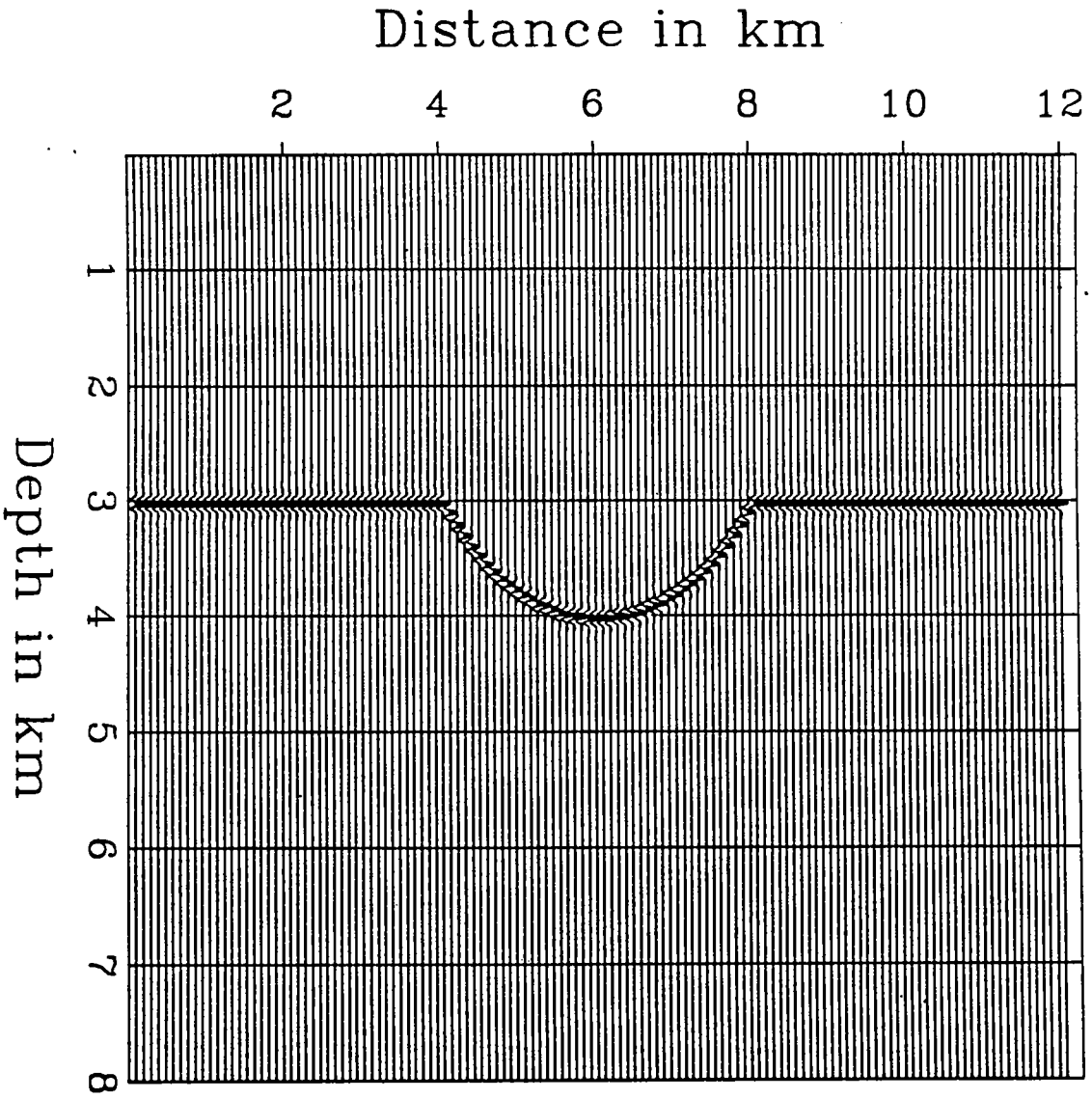

Figure 12. Synthetic model.

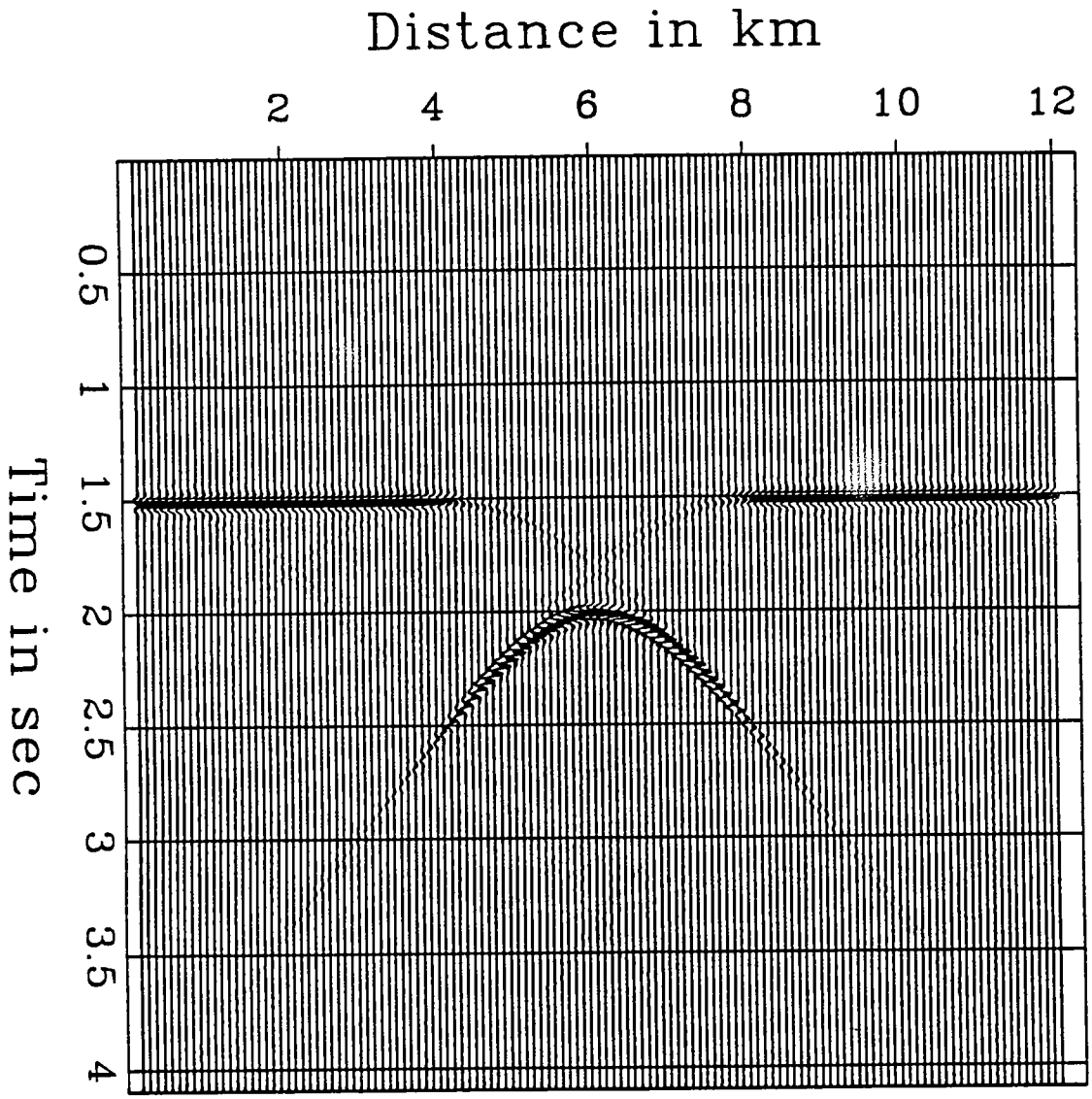

Figure 13. Synthetic zero-offset data.

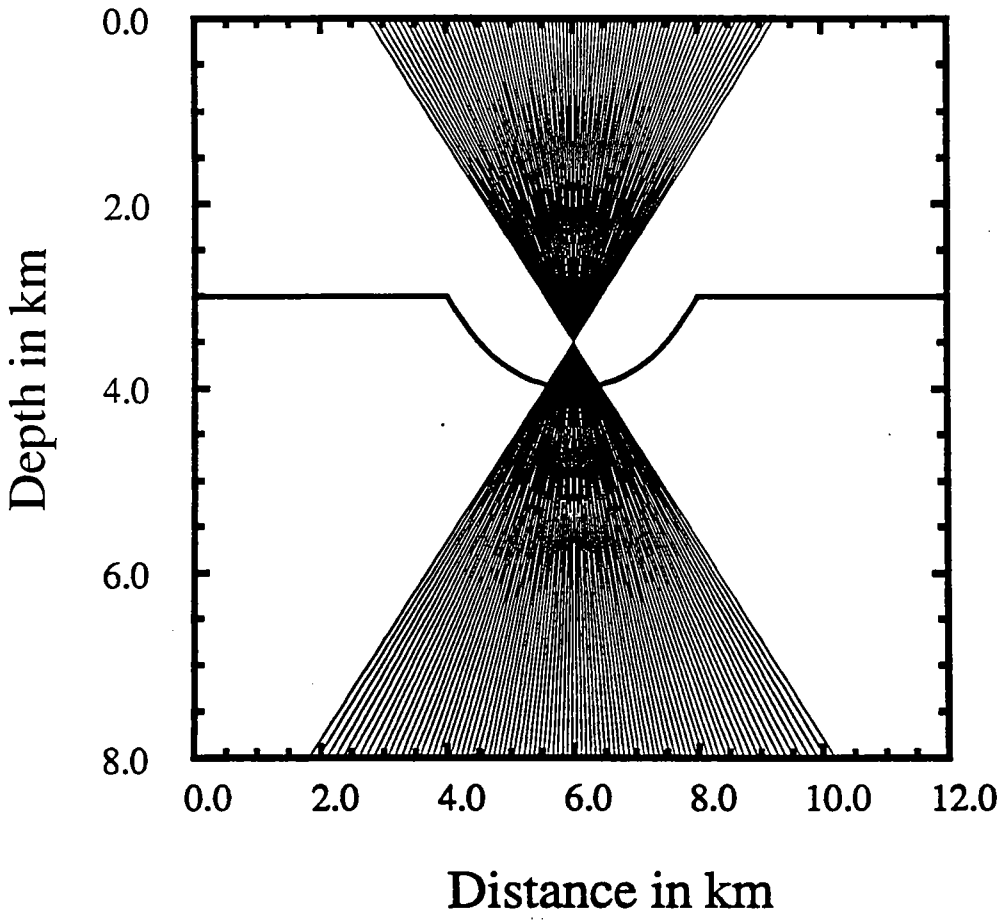

Figure 14. Rays used for imaging.

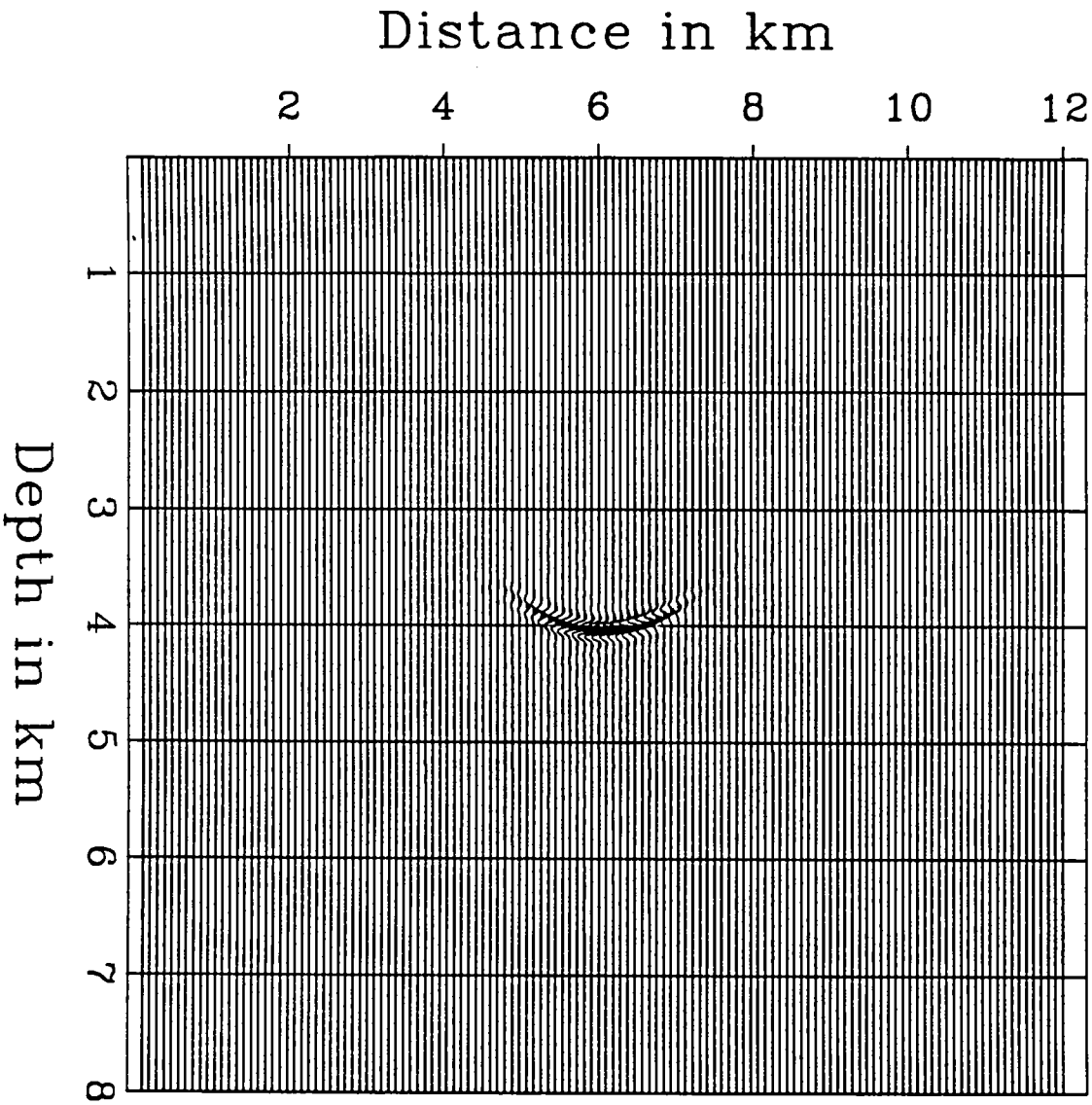

Figure 15. Image constructed from rays shown in Figure 14.

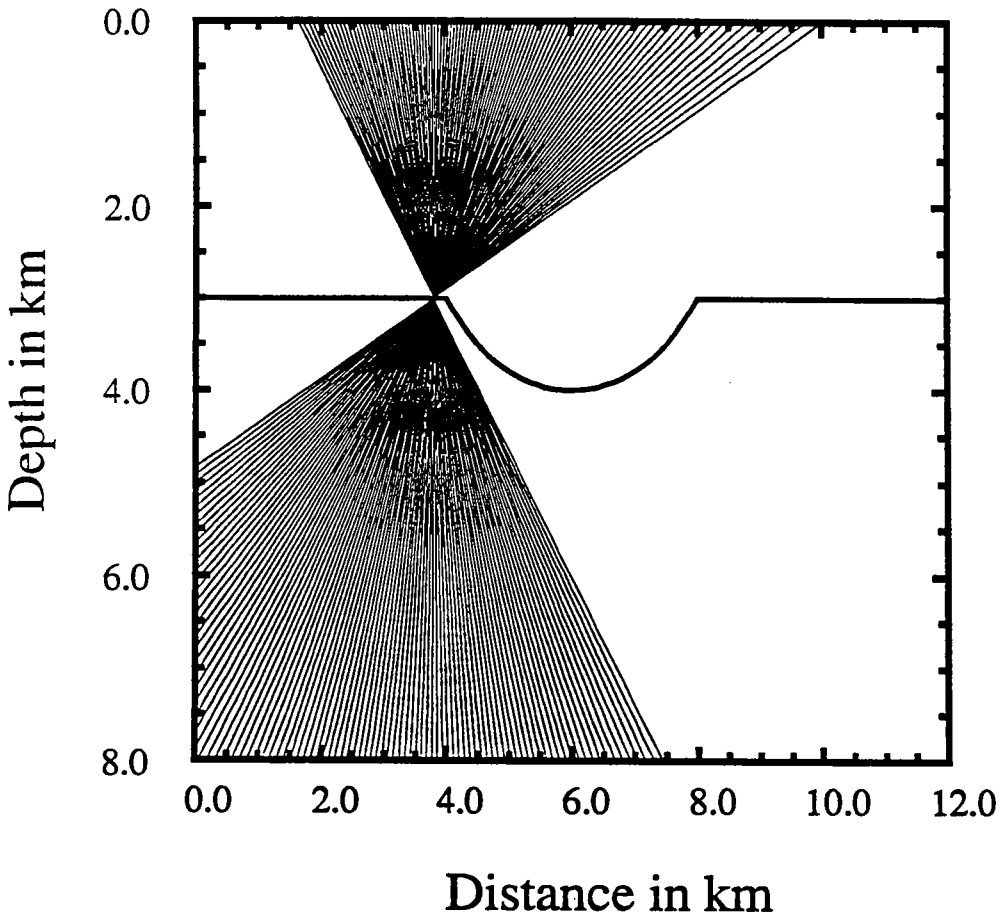

Figure 16. Rays used for imaging.

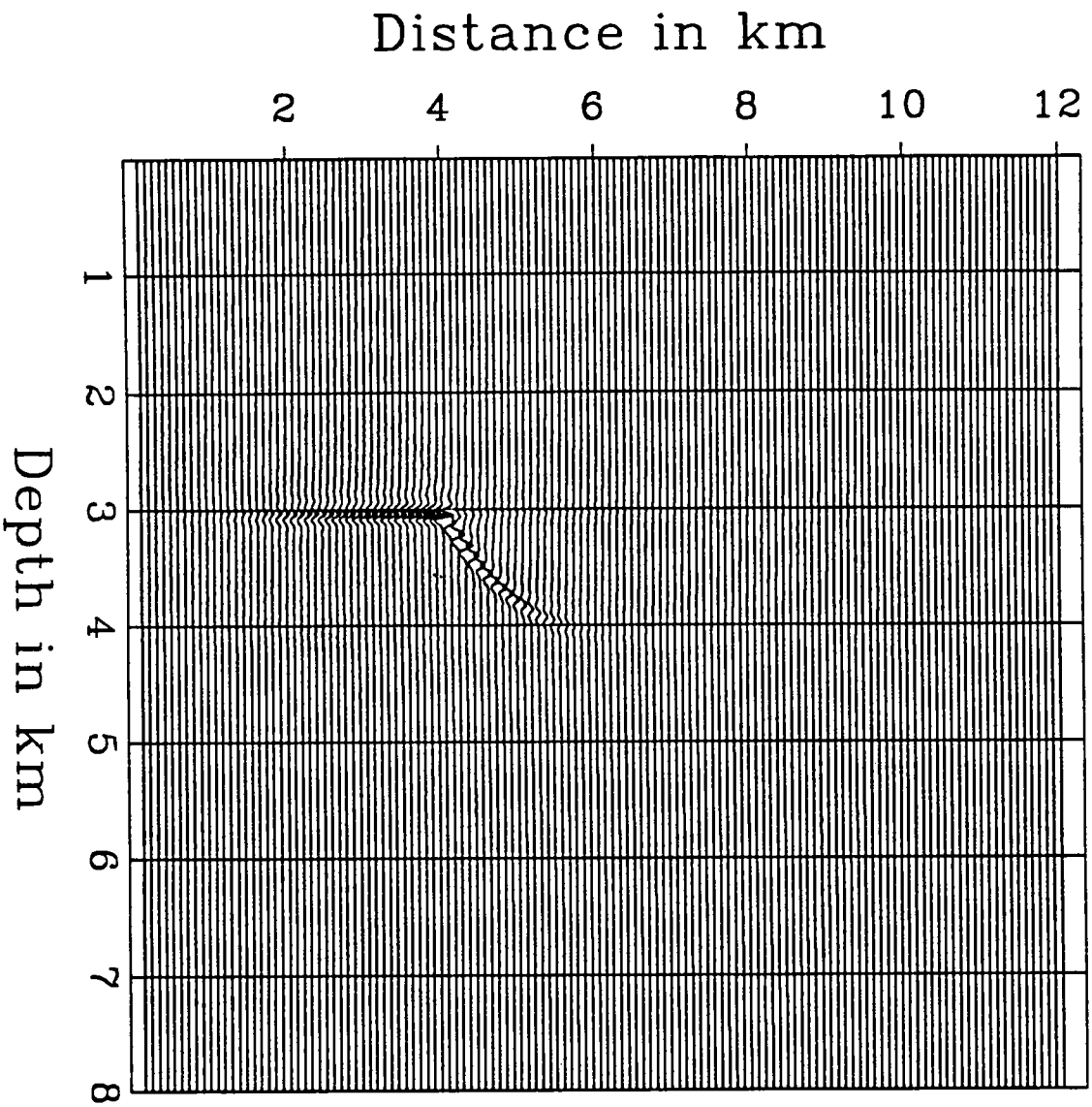

Figure 17. Image constructed from rays shown in Figure 16.

of migration like finite-difference migrations.

2. Flexibility in the choice of imaging parameters. Some of the parameters that can be selected are:

- Beam widths and positions of ray fans.
- Range of dips to be imaged. Some dips might be associated with noise. We might want to image a few dips at a time (like for example in the case of VSP migrations and VSP-CDP transformations). It is often the case that several migrations will be performed, in order to select the optimal velocity model that will produce a well focused image. In this case an estimate of the local dip will be available after the first migration. In subsequent migrations we could just image a small range of dips around the main local dip. Since the cost of our migration is proportional to the number of dips we are migrating for, these subsequent migrations could be performed very efficiently.
- Sampling rate. Steep dips might need higher sampling rates to avoid aliasing artifacts, while coarser sampling might perform satisfactorily for small dips.
- Range of offsets used in prestack migration. Information about a reflector can be extracted from all available angles of incidence or from a subset of them. We might want to use the AVO information in different ways for different ranges of incidence angle. For example, we may want to separate pre- and post-critical reflections, small from large offsets etc.

The choice of these parameters could be different for different areas.

3. Optimization of velocity model. Probably the most difficult problem associated with imaging is not how to migrate correctly given a velocity model. It is how to define this velocity model. Or, given an imperfectly focused migrated image, how should we update the velocity model to achieve better focusing?

Prestack migration could be used as a tool for velocity analysis. The underlying idea is that, if the velocity model is correct, the images obtained from different offsets should be the same independent of structure. This is a very active field of current research activity.

Consider an area that we want to image. Suppose the condition for optimal focusing stated above can be expressed as the maximization of an objective function (Denelle, Trézéguet and Tarantola (1987)). To maximize the objective function through some of the classic optimization methods we will need to calculate its gradient with respect to the velocity model. Our imaging approach should provide us with an efficient way to calculate this gradient.

Look at the situation shown schematically in Figure 18. Ray 1 has a well defined contribution to the image of the target area: this contribution is calculated by summing the data along the stacking trajectories A and spreading the result along the spreading trajectories P. If the velocity model changes, Ray 1 is going to change into Ray 2 (we keep the initial angle of the ray the same to keep the same spreading

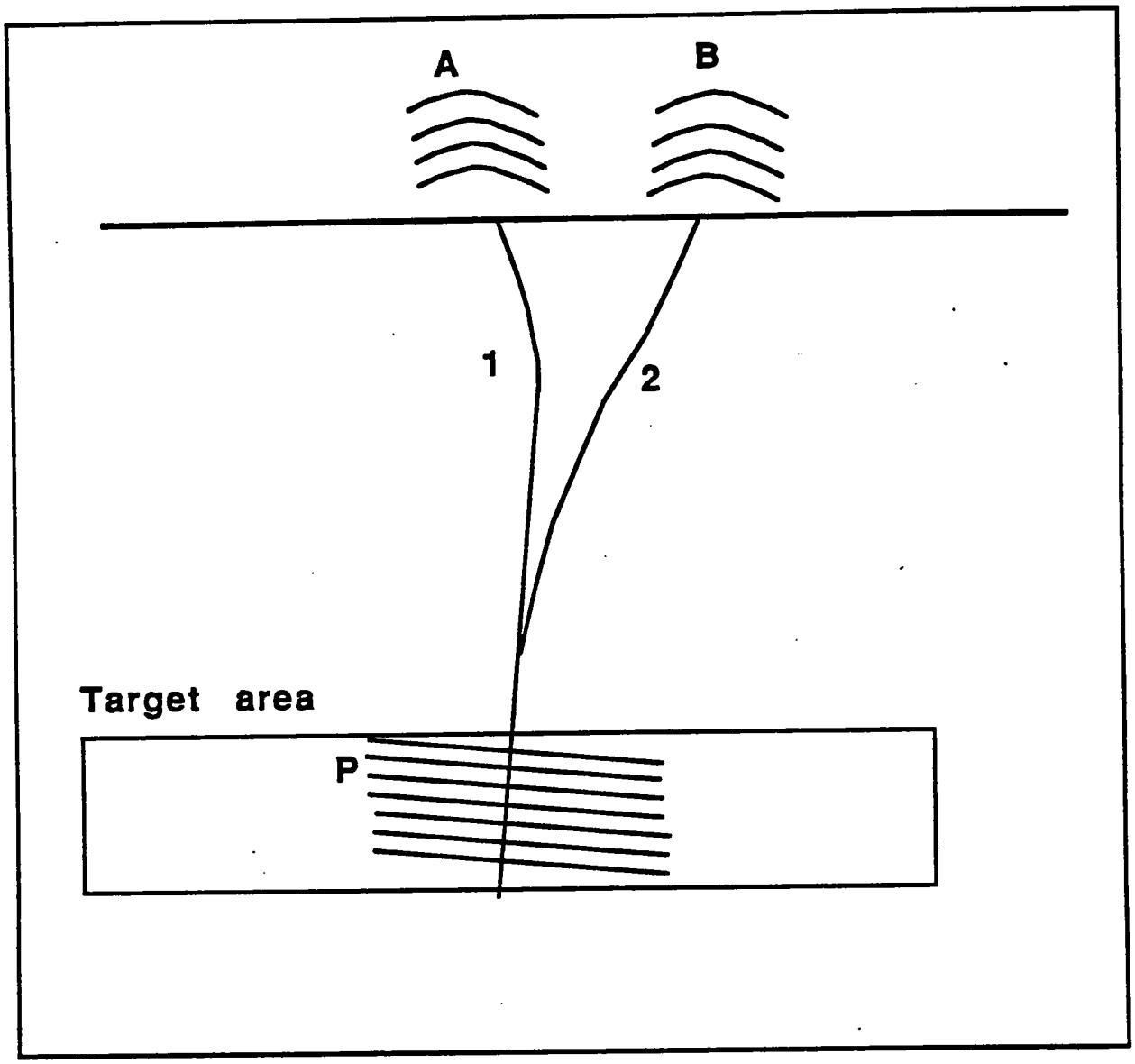

Figure 18. Change of the image of a target area due to a change in a ray.

trajectories). The stacking trajectories A are replaced by the stacking trajectories B. So, to calculate the change in the image due to the change in the model which produced this particular ray perturbation, we just have to do the following:

1. Stack along the old stacking trajectories and spread the result along P with a negative sign (to eliminate the effect of the old stacking trajectories on the image).

2. Stack along the new stacking trajectories and spread the result along P with a positive sign.

For small perturbations this procedure will essentially be the calculation of the gradient. This gradient can be described as a chain of two effects: the change of the raypath due to a perturbation in the velocity model and the change of the result of the stacking due to a perturbation in the stacking trajectories. The first part can be calculated by a slightly more expensive ray tracing. The second part is completely data dependent. It can be calculated by finite difference operations on the data.

Obviously the ability of our algorithm to image with relatively few rays is very important, since the connection between image and velocity model is established in an efficient way. It is also important that the effect of each ray on the image is well defined through the use of the Radon transform, since this allows for a well defined gradient. The ability of the algorithm to concentrate on specific dips is significant as well, since the iterative migrations could be performed efficiently, imaging a small range of dips around the dominant local dip.

4. Born inversion Born inversion uses the amplitude vs. offset information to produce estimates of the high wavenumbers of the elastic properties of the subsurface (P-wave velocity, S-wave velocity, density). In Lazaratos (1989) we showed how to perform a Kirchoff type elastic Born inversion and Gaussian beam elastic Born inversion by combining the outputs of three slightly different migrations.

5. 3-D. This is too far down the road yet. Still, it is safe to predict that algorithms that can concentrate on areas of interest and optimize their imaging would be of even greater significance in 3-D.

CONCLUSION

We presented a new migration algorithm. It is based on the synthesis of an image from its dip spectrum. The calculation of this spectrum is performed by stacking operators, defined through Gaussian beams. Some initial experiments with simple zero-offset synthetic examples have been encouraging. Still further testing with more complicated models and real data is needed, particularly for the prestack version of the algorithm. The new migration provides the ability to efficiently image regions of interest with significant flexibility in the choice of the imaging parameters. It might have important applications in migration velocity optimization and Born inversion.

REFERENCES

Berkhout, A. J., 1981, Wave field exptrapolation techniques in seismic migration, a tutorial: Geophysics, **46**, 1638-1656.

Beydoun, W. B., and Keho, T. H., 1987, The paraxial ray method: Geophysics, **52**, 1639-1653.

Beydoun, W. B., and Mendes, M., 1989, Elastic ray-Born l_2-migration/inversion: Geophysical Journal, **97**, 151-160.

Beylkin, G., 1985, Imaging of discontinuities in the inverse scattering problem by inversion of a causal generalized Radon transform: J. Math. Phys., **26**, 99-108.

Beylkin, G., and Burridge, R., 1987, Multiparameter inversion for acoustic and elastic media, in Expanded Abstracts of 57th Annual International SEG Meeting, Society of Exploration Geophysicists, New Orleans, 747-749.

Bleistein, N., 1987, On the imaging of reflectors in the earth: Geophysics, **52** 931-942.

Bleistein, N., Cohen, J. K., and Hagin, F. G., 1985, Computational and asymptotic aspects of velocity inversion: Geophysics, **52**, 26-36.

Carter, J. A., and Frazer, L. N., 1984, Accommodating lateral velocity changes in Kirchoff migration by means of Fermat's principle: Geophysics, **49**, 46-63.

Červený, V., 1983, Synthetic body wave seismograms for laterally varying layered structures by the Gaussian beam method: Geoph. J. R. Astr. Soc., **73**, 389-426.

Červený, V., 1985, The application of ray tracing to the propagation of shear waves in complex media: Handbook of Geophysical Exploration, Vol. 15A, Seismic Shear Waves, Helbig K. and Treitel S., eds, 1-124.

Červený, V., 1985a, Gaussian beam synthetic seismograms: Journal of Geophysics, **58**, 44-72.

Červený, V., and Pšenčik, I., 1983, Gaussian beam and paraxial ray approximation in three-dimensional elastic inhomogeneous media: Journal of Geophysics, **53**, 1-15.

Červený, V., Popov, M. M., and Pšenčik, I., 1982, Computation of wave fields in inhomogeneous media - Gaussian beam approach: Geoph. J. R. Astr. Soc., **70**, 109-128.

Claerbout, J. F., 1984, Imaging the Earth's interior: Blackwell Scientific Publications Ltd.

Clayton, R. W., and Stolt, R. H., A Born - WKBJ inversion method for acoustic reflection data: Geophysics, **46**, 1559-1567.

Cohen, J. K., Hagin, F. G., and Bleistein, N., 1986, Three-dimensional Born inversion with an arbitrary reference: Geophysics, **51**, 1552-1558.

Costa, C. A., Raz, S., Kosloff, D., 1989, Gaussian beam migration, in Expanded Abstracts of 59th Annual International SEG Meeting, Society of Exploration Geo-

physicists, Dallas, 1169-1171.

Deans, S. R, 1983, The Radon transform and some of its applications, J. Wiley and Sons, Inc.

Denelle, E., Trézéguet, D., and Tarantola, A., 1987, Nonlinear inversion by depth extrapolation in the shots-geophones domain, in Expanded Abstracts of 57th Annual International SEG Meeting, Society of Exploration Geophysicists, New Orleans, 753-754.

Devaney, A. J., 1984, Geophysical diffraction tomography: IEEE Trans. on Geoscience and Remote Sensing, **22**, 3-13.

Gabor, D., 1946, Theory of communication: J. Inst. Electr. Electron. Eng. (London), **93 III**, 429-491.

Harris, J. M., 1987, Diffraction tomography with arrays of discrete sources and receivers: IEEE Trans. on Geoscience and Remote Sensing, **25**, 448-455.

Hildebrand, S., and Carroll, R., Slant-stack depth migration: dynamic ray theory approach, in Expanded Abstracts of 59th Annual International SEG Meeting, Society of Exploration Geophysicists, Dallas, 1190-1191.

Ikelle, L. T., 1989, GRT Inversion: Practical Aspects, in Expanded Abstracts of 59th Annual International SEG Meeting, Society of Exploration Geophysicists, Dallas, 1009-1012.

Keho, T. H., and Beydoun, W. B., 1988, Paraxial ray Kirchoff migration: Geophysics, **53**, 1540-1546.

Klimeš, L., 1984, Expansion of a high frequency time-harmonic wavefield given on an initial surface into Gaussian beams: Geoph. J. R. Astr. Soc., **79**, 105-118.

Lazaratos, S., 1989, Gaussian beam inversion for cross-borehole seismic data, in Stanford Rock and Borehole Project, Rep. No. 37, I1-66.

Miller, D., Oristaglio, M., and Beylkin, G., 1987, A new slant on seismic imaging: Migration and integral geometry: Geophysics, **52**, 943-964.

Radon, J., 1917, Über die Besttimmung von Funktionen durch ihre Integralwerte längs gesisser Mannigfaltigkeiten: Ber., Verh. Sächs. Akad., **69**, 262-277.

Raz, S., 1987, Beam stacking: a generalized preprocessing technique: Geophysics, **52**, 1199-1210.

Schneider, W. A., 1978, Integral formulation for migration in two and three dimensions: Geophysics, **43**, 49-76.

Stolt, R. H., and Weglein, A. B., 1985, Migration and inversion of seismic data: Geophysics, **50**, 2458-2472.

APPENDIX A - FAR FIELD, HIGH FREQUENCY APPROXIMATION OF KIRCHOFF INTEGRAL

In this appendix we show that equation (12) is an approximate form of equation (10). In the far field and for high frequencies the wavefield $W_{\vec{p},l}(\vec{r}_R;\omega)$ can be approximated locally by a plane wave propagating at the direction of the normal to the wavefront. So, under these approximations

$$W_{\vec{p},l}(\vec{r}_R;\omega) \simeq A(\vec{r}_R)\exp[i\frac{\omega}{v(\vec{r}_R)}(x\sin\theta(\vec{r}_R) - z\cos\theta(\vec{r}_R)] \tag{29}$$

In this equation $A(\vec{r}_R)$ is a geometric spreading factor, $\theta(\vec{r}_R)$ is the angle between the vertical and the normal to the wavefront and $v(\vec{r}_R)$ the velocity at the receiver location $\vec{r}_R$. All three are assumed to be very slowly varying functions of $\vec{r}_R$.

The first term of the integral in equation (10) is

$$\int d\vec{r}_R U_s(\vec{r}_R;\omega)\frac{\partial W_{\vec{p},l}(\vec{r}_R;\omega)}{\partial z_R} \equiv \int dx U_s(x;\omega)\frac{\partial W_{\vec{p},l}(x,z=0;\omega)}{\partial z} \tag{30}$$

since the receivers are on the line $z = 0$. Using the inverse Fourier transform expression for $U_s(x;\omega)$ and interchanging the order of the integrations we can write this term as:

$$\frac{1}{2\pi}\int dk_x \int dx U_s(k_x;\omega)A(\vec{r}_R)[-i\frac{\omega}{v(\vec{r}_R)}\cos\theta(\vec{r}_R)]\exp\{i[k_x + \frac{\omega}{v(\vec{r}_R)}\sin\theta(\vec{r}_R)]x\} \tag{31}$$

Using the fact that

$$\frac{\partial U_s(x;\omega)}{\partial z} = \frac{1}{2\pi}\int dk_x U_s(k_x;\omega)[i\frac{\omega}{v(\vec{r}_R)}\sqrt{1 - k_x^2 v^2(\vec{r}_R)/\omega^2}]\exp(ik_x x) \tag{32}$$

the second term in equation (10) can be written as

$$\frac{1}{2\pi}\int dk_x \int dx U_s(k_x;\omega)A(\vec{r}_R)[i\frac{\omega}{v(\vec{r}_R)}\sqrt{1 - k_x^2 v^2(\vec{r}_R)/\omega^2}]\exp\{i[k_x + \frac{\omega}{v(\vec{r}_R)}\sin\theta(\vec{r}_R)]x\} \tag{33}$$

It can be easily shown that the stationary phase approximations of the expressions in equations (31) and (33) are the same with opposite signs. So, the Kirchoff integral of equation (10) can be approximated with twice the quantity

$$\int d\vec{r}_R U_s(\vec{r}_R;\omega)\frac{\partial W_{\vec{p},l}(\vec{r}_R;\omega)}{\partial z_R} \tag{34}$$

where, according to equation (29)

$$\frac{\partial W_{\vec{p},l}(\vec{r}_R;\omega)}{\partial z_R} = -i\omega\frac{\cos\theta(\vec{r}_R)}{v(\vec{r}_R)}W_{\vec{p},l}(\vec{r}_R;\omega) \tag{35}$$

Substituting this last expression into equation (34) we end up with the right-hand side integral in equation (12).

APPENDIX B - DETERMINATION OF THE COEFFICIENTS FOR THE GAUSSIAN BEAM DECOMPOSITION

We demonstrate here how to calculate the coefficients for the expansion of $f(\vec{r})$ into the basis defined by the Gaussian beam wavefields $B_{i,\vec{p},l}(\vec{r})$. The expansion is of the form

$$f'(\vec{r}) = \sum_i \sum_{\vec{p}} \sum_l a_{i,\vec{p},l} B_{i,\vec{p},l}(\vec{r}) \tag{36}$$

where

$$f(\vec{r}) = R(\vec{r}) * f'(\vec{r}) \tag{37}$$

and $R(\vec{r})$ is the two-dimensional rho-filter. We determine the coefficients $a_{i,\vec{p},l}$ by minimizing the error

$$\int d\vec{r} |f'(\vec{r}) - \sum_i \sum_{\vec{p}} \sum_l a_{i,\vec{p},l} B_{i,\vec{p},l}(\vec{r})|^2 \tag{38}$$

Minimizing this objective function leads to a system of equations

$$Ax = y \tag{39}$$

where x is the vector of unknown coefficients $a_{i,\vec{p},l}$ and y is the vector consisting of the elements

$$\int d\vec{r} f'(\vec{r}) B_{i,\vec{p},l}(\vec{r}) \tag{40}$$

This quantity is the value of the convolution of the spatial functions $f'(\vec{r})$ and $B_{i,\vec{p},l}(-\vec{r})$ at $\vec{r} = 0$. The function $f'(\vec{r})$ is the convolution of $f(\vec{r})$ and the inverse of the rho-filter. Instead of applying the inverse rho-filter on $f(\vec{r})$, we can apply it on $B_{i,\vec{p},l}(\vec{r})$. So the elements of y can be written as

$$\int d\vec{r} f(\vec{r}) B'_{i,\vec{p},l}(\vec{r}) \tag{41}$$

where

$$B_{i,\vec{p},l}(\vec{r}) = R(\vec{r}) * B'_{i,\vec{p},l}(\vec{r}) \tag{42}$$

The elements of the matrix A are

$$\int d\vec{r} B_{i,\vec{p},l}(\vec{r}) B_{i',\vec{p}',l'}(\vec{r}) \tag{43}$$

The matrix A is close to being diagonal. Keeping only the diagonal terms we simply have

$$a_{i,\vec{p},l} = c^{-1} \int d\vec{r} f(\vec{r}) B'_{i,\vec{p},l}(\vec{r}) \tag{44}$$

where the constant c is

$$c = \int d\vec{r} B^2_{i,\vec{p},l}(\vec{r}) \tag{45}$$

So the final result is

$$f(\vec{r}) = R(\vec{r}) * \sum_i \sum_{\vec{p}} \sum_l B_{i,\vec{p},l}(\vec{r}) \int d\vec{r} f(\vec{r}) B'_{i,\vec{p},l}(\vec{r}) \tag{46}$$

The constant c is omitted, since it produces no effect on the migrated image.